Synthesis, Structure, and Properties of 4,8,12-Trioxa-12c-phospha-4,8,12,12c-tetrahydrodibenzo-[*cd*,*mn*]pyrene, a Molecular Pyroelectric

Frederik C. Krebs,* Peter S. Larsen, Jan Larsen, Claus S. Jacobsen,[†] Carlo Boutton,[‡] and Niels Thorup[§]

Contribution from the Macromolecular Chemistry Group, Department of Solid State Physics, Risø National Laboratory, DK-4000 Roskilde, Denmark

Received June 17, 1996. Revised Manuscript Received November 5, 1996[⊗]

Abstract: The title compound (**4**) was synthesized, and its crystalline structure was determined. The molecule has C_{3v} point symmetry and crystallizes in the trigonal space group *R*3*m*. Crystal data for **4**: $a = 16.6710(13)$ Å, $b = 16.6710(13)$ Å, $c = 4.2590(3)$ Å, $\alpha = \beta = 90°$, $\gamma = 120°$, $Z = 3$, $R(F) = 0.0234$. The material has a permanent polarization and consequent pyroelectric properties. The room temperature pyroelectric coefficient was found to be -3 ± 2 μC m^{-2} K^{-1}, which is in accordance with a calculated value of -3.2 μC m^{-2} K^{-1}. The molecular dipole moment was determined to be 3.3 ± 0.2 D, the direction of which was unambiguously assigned with respect to the molecular coordinates. The thermal expansivity was determined at temperatures in the range −93 to 200 °C. The relative dielectric permittivity tensor was obtained at optical frequencies (ϵ_{11} and $\epsilon_{22} = 3.16$ and $\epsilon_{33} = 2.48$) and in the microwave region at 35 GHz (ϵ_{11} and $\epsilon_{22} = 5.2 \pm 0.6$ and $\epsilon_{33} = 2.9 \pm 0.2$), and at low frequencies (120 Hz and 1 kHz), the isotropic permittivity was determined ($\epsilon_{120\ \mathrm{Hz}} = 4.7 \pm 0.8$ and $\epsilon_{1\ \mathrm{kHz}} = 4.7 \pm 1.1$). Finally, an estimate of the molecular heat capacity was calculated ($C_p = 900$ J Kg^{-1} K^{-1}) and the material was considered for potential use in infrared detection as its detectivity merit factor, M_r, was determined ($M_r = 8.8 \times 10^{-2}$ m^2 C^{-1}).

Introduction

Materials exhibiting pyroelectric properties are used as the active components in infrared detectors,[1−4] in infrared video cameras,[5,6] in pyroelectric image tubes,[7] and in the formation of pyro-electrooptic transient gratings,[8] to mention only a few areas of application. From a materials science point of view, there is thus an interest in developing new materials where better performance can be achieved with respect to detectivity, ease of incorporation in devices, compatibility with known technology, etc. There is however also a fundamental interest in obtaining materials in which the nature of the pyroelectric effect can be controlled. This essentially implies the development of a deeper understanding of the phenomenon. The pyroelectric effect itself is observed in molecular materials,[9−18] inorganic/organic salts,[19−27] inorganic/ceramic materials,[20,25−35] polymers,[5,6] and liquid crystals.[36] Various approaches have been employed in attempting to control the nature of the pyroelectric effect depending on the area of chemistry from which the pyroelectric material stems. The majority of known pyroelectric materials fall within the category of inorganic/ceramic materials, and the approach to control the pyroelectric effect in this respect has been by doping and varying composition without affecting the structure[3,31,32] and by development of solid solution systems,[35] and also, the effect of the crystal growth method has been investigated.[34] The inorganic/organic salts are typically

[†] Department of Physics, Technical University of Denmark, DK-2800 Lyngby, Denmark.
[‡] Laboratorium voor Chemische en Biologische Dynamica, Celestijnenlaan 200D, B-3001 Heverlee, Belgium.
[§] Department of Chemistry, Technical University of Denmark, DK-2800 Lyngby, Denmark.
[⊗] Abstract published in *Advance ACS Abstracts,* January 15, 1997.

(1) Glass, A. M. *Appl. Phys. Lett.* **1968**, *13*, 147−149.
(2) Byer, R. L.; Roundy, C. B. *Ferroelectrics* **1972**, *3*, 333−338.
(3) Glass, A. M. *J. Appl. Phys.* **1969**, *40*, 4699−4713.
(4) Liu, S. T.; Maciolek, R. B. *J. Electron Mater.* **1975**, *4*, 91−100.
(5) Dubois, J. C. *Mol. Cryst. Liq. Cryst.* **1994**, *255*, 231−242.
(6) Robin, P.; Facoetti, J. C.; Dubois, C.; Dautriche, P.; Pourquier, E. *Onde Electr.* **1994**, *74*, 34−36.
(7) Taylor, R. G.; Boot, A. H. *Contemp. Phys.* **1973**, *14*, 55−87.
(8) Ducharme, S. *Optics Lett.* **1991**, *16*, 1791−1793.
(9) Koptsik, V. A. *Sov. Phys. Crystallogr.* **1960**, *4*, 197−200.
(10) Gavrilova, N. D. *Sov. Phys. Crystallogr.* **1965**, *10*, 91−92.
(11) Sworakowski, J. *Molecular Electronics*; Ashwell, G. J., Ed.; Research Studies Press Ltd.: John Wiley & Sons, England, 1992; pp 266−331.
(12) Terauchi, H.; Kojima, T.; Sakaue, K.; Tajiri, F. *J. Chem. Phys.* **1982**, *76*, 612−615.
(13) Giermanska, J.; Nowak, R.; Sworakowski, J. *Ferroelectrics* **1985**, *65*, 165.
(14) Lang, S. B.; Cohen, M. D.; Steckel, F. *J. Appl. Phys.* **1965**, *36*, 3171−3173.
(15) Gavrilova, N. D.; Drozhdin, S. N.; Novik, V. K.; Maksimov, E. G. *Solid State Commun.* **1983**, *48*, 129−133.
(16) Asaji, T.; Weiss, A. *Z. Naturforsch.* **1985**, *40a*, 567−574.
(17) Fleck, S.; Weiss, A. *Z. Naturforsch.* **1987**, *42a*, 645.
(18) Asaji, T.; Taya, M.; Nakamura, D. *Phys. Status Solidi A* **1987**, *102*, 815−818.
(19) Zheludev, I. S.; Gladkii, V. V. *Sov. Phys. Crystallogr.* **1966**, *11*, 366−368.
(20) Simhony, M.; Shaulov, A. *J. Appl. Phys.* **1971**, *42*, 3741.
(21) Unruh, H. -G. *Solid State Commun.* **1970**, *8*, 1951−1954.
(22) Nomura, S. *J. Phys. Soc. Jpn.* **1961**, *16*, 2440−2452.
(23) Lang, S. B. *Phys. Rev. B* **1971**, *4*, 3603−3609.
(24) Ackermann, W. *Ann. Phys.* **1915**, *46*, 197−230.
(25) Gladkii, V. V.; Zhedulev, I. S.; Sidnenko, E. V. *Bull. Acad. Sci. USSR, Phys. Ser.* **1969**, *33*, 276−281.
(26) Novik, V. K. *Sov. Phys. Crystallogr.* **1965**, *10*, 89−90.
(27) Sawada, S.; Nomura, S.; Asao, Y. *J. Phys. Soc. Jpn.* **1961**, *16*, 2207−2212.
(28) Röntgen, W. C. *Ann. Phys.* **1914**, *45*, 737−800.
(29) Savage, A. *J. Appl. Phys.* **1966**, *37*, 3071−3072.
(30) Heiland, G. Ibach, H. *Solid State Commun.* **1966**, *4*, 353−356.
(31) Liu, S. T.; Heaps, J. D.; Tufte, O. N. *Ferroelectrics* **1972**, *3*, 281−285.
(32) Liu, S. T.; Kyonka, J. *Ferroelctrics* **1974**, *7*, 167−169.
(33) Thatcher, P. D. *J. Appl. Phys.* **1968**, *39*, 1996−2002.
(34) Wemple, S. H.; Didomenico Jr., M.; Camlibel, I. *J. Phys. Chem. Solids* **1968**, *29*, 1797−1803.
(35) Iwasaki, H.; Miyazawa, S.; Koizumi, H.; Sugii, K.; Niizeki, N. *J. Appl. Phys.* **1972**, *43*, 4907−4915.
(36) Tournilhac, F.; Blinov, L. M.; Simon, J.; Subachius, D. B.; Yablonsky, S. V. *Synth. Met.* **1993**, *54*, 253−261.

S0002-7863(96)02023-9 CCC: $14.00

salts of organic or inorganic acids, where the approach has been to observe the effect of exchanging the cations,[24] but also, the effect of experimental conditions like crystal growth temperature has been investigated.[37] Within the polymeric pyroelectrics, the approach has been to substitute halogen atoms and copolymerize similar monomers.[5,6,38] The liquid crystalline approach has been to control chirality and composition of binary mixtures of polyphillic molecules.[36] Up until 1983 few purely molecular organic pyroelectric materials were known and characterized;[9,10] from this date, however, systematic studies on the pyroelectricity of molecular materials began[11] and quite a few molecular pyroelectrics are known and characterized today.[12−18] Many of these materials stem from *meta*-substituted benzene derivatives[13−18] as these derivatives have a pronounced tendency to crystallize in a polar space group.[39] In order for a molecular material to exhibit pyroelectric properties, the molecule itself must have a permanent dipole moment and it must crystallize in one of the 10 pyroelectric point groups.[40] While most organic molecules possess a permanent dipole moment, few crystallize in one of the pyroelectric point groups.[41,42] We have synthesized and crystallized the molecule **4** which differs from most other molecular pyroelectrics by having a high molecular symmetry and not showing strong intermolecular interactions as evidenced by sublimation at temperatures just above room temperature. The molecular material **4** investigated in this paper is built from this simple symmetrical molecule with a particular shape that implies the presence of a permanent dipole moment and, at the same time, allows the molecules to stack, the consequence of which may be reflected in the exceptionally clear and simple crystal structure that enables one to see directly that the material is polarized. The molecular dipole moment vector coincides with the molecular C_3 axis, which again coincides with the polar axis of the crystal. The nature of the pyroelectric effect as observed from 28 to 110 °C can be developed by the combination of a measurable molecular property, the dipole moment, and the crystalline structural properties, the molecular arrangement and the thermal expansivity.

When considering a material for use as the active component in a detector system, it is important that its ability to detect a given signal can be expressed in a manner such that a comparison with other materials is possible. The way to achieve this is by deriving a merit factor[1−7,31] which takes into account certain physical properties pertaining to the material and some physical factors pertaining to the geometry and construction of the detector in question. The physical factors which depend solely upon the material are the dielectric constant, the density, the heat capacity, the themal conductivity,[7] the loss tangent,[4,31] and of course the pyroelectric coefficient. The physical factors which depend upon the geometry and construction are the thickness and the area of the detector material in the actual detector system, the assocciated electrical capacitance[2,3] of the detector crystal with electrodes, and the frequency at which detection is done. The physical factors having an influence on the magnitude of the merit factor therefore depend upon the disposition of the chosen detector system, for instance, whether it is time dependent or time independent, whether potential or charge is read,[5,6] or whether it is a low-noise detector system.[7] A large detector response to a given energy input is not solely granted by a large pyroelectric coefficient. Other factors which interplay are the density, dielectric constant along the polar axis, and the heat capacity, which all have to be small in value to get a large response. This is because the magnitude of the detector response is directly proportional to the pyroelectric coefficient but inversely proportional to the latter three quantities. The main advantage of molecular materials in this respect is that even though their pyroelectric coefficient often is only moderate in magnitude the value of their relative dielectric constant is rarely above 10.[40] Many inorganic/ceramic materials have large pyroelectric coefficients but often relative dielectric constants with values in excess of several hundred.[40] The pyroelectric coefficient and the dielectric constant therefore often balance each other with respect to the magnitude of the detectivity merit factor. Another advantage of molecular materials is of course their low density compared to that of most inorganic/ceramic materials. The heat capacity of molecular materials however is usually comparable to slightly higher in value than the corresponding inorganic/ceramic materials. In this paper a time and physical disposition independent detectivity merit factor, M_r, for compound **4** was evaluated so that the material could be compared with other known materials without considering how an actual detector system should be constructed.

Experimental Section

Synthetic Methods and Materials. All reagents used were standard grade unless otherwise mentioned. THF was dried by distillation from Na/benzophenone under argon. NMP was dried by distillation from CaH_2 under vacuum. NMR spectra were recorded on a 250 MHz BRUKER NMR spectrometer. ^{31}P-NMR spectra were recorded with a capillary containing 85% H_3PO_4(aq) as a reference. Melting points were determined using a BÜCHI melting point apparatus or if stated determined by DSC on a Perkin Elmer DSC-4. Mass spectra were determined using a JEOL JMS HX110-110T mass spectrometer. Elemental analysis was done at the University of Copenhagen, Department of Chemistry, Elemental Analysis Laboratory, Universitetsparken 5, 2100 Copenhagen, Denmark.

1-[2-Tetrahydropyranyl)oxy]-3-fluorobenzene (1). 3-Fluorophenol (75 g, 0.669 mol) and dihydropyran (79 g, 0.928 mol) were mixed in a 500 mL conical flask while being cooled to a temperature of −35 °C in a CO_2(s)/acetone bath. The cooling was removed, and the solution was stirred while 37% HCl(aq) (1 mL) was added. The temperature was allowed to rise while the solution was stirred. After 15 min, the reaction took place, and the mixture acquired room temperature and was stirred for one-half hour, during which crystallization occurred. Ether (500 mL) was added, and the organic layer was washed with 1 M $NaHCO_3$(aq) (200 mL) and dried (Na_2SO_4). The ether was evaporated on a rotary evaporator, and the crude oil was crystallized by dissolution in boiling hexane (200 mL) followed by cooling. This gave **1** (110 g, 83%) as colorless crystals: mp 47−48 °C; ^{1}H-NMR ($CDCl_3$) δ 7.26−7.14 (m, 1H), 6.82 (td, 1H, $J_1 = 6.0$ Hz, $J_2 = 2.2$ Hz, $J_3 = 0.6$ Hz), 6.79 (dt, 1H, $J_1 = 11.3$ Hz, $J_2 = 2.2$ Hz), 6.67 (tdd, 1H, $J_1 = 8.5$ Hz, $J_2 = 2.5$ Hz, $J_3 = 1$ Hz,), 5.38 (t, 1H, $J = 3.1$ Hz), 3.93−3.82 (m, 1H), 3.65−3.55 (m, 1H), 2.1−1.5 (m, 6H); ^{13}C-NMR ($CDCl_3$) δ 163.91 (d, $J = 245.2$ Hz), 158.81 (d, $J = 10.9$ Hz), 130.43 (d, $J = 9.7$ Hz), 112.54 (d, $J = 3$ Hz), 108.69 (d, $J = 21.2$ Hz), 104.56 (d, $J = 24.8$ Hz), 96.95 (s), 62.42 (s), 30.63 (s), 25.52 (s), 19.06 (s) Anal. Calcd for $C_{11}H_{13}FO_2$: C, 67.33; H, 6.67. Found: C, 67.20; H, 6.67.

Tris[[(2-tetrahydropyranyl)oxy]-6-fluorophenyl]phosphine (2). 1 (12 g, 61.1 mmol) was dissolved in dry THF (250 mL). The solution was cooled to −78 °C on a CO_2(s)/acetone bath under argon. *n*-BuLi (1.6 M, 38.2 mL, 61.1 mmol) was added, and the reaction mixture was stirred for one-half hour. PBr_3 (1.78 mL, 19 mmol) was added. After the mixture stirred for 1 h, the reaction was quenched with MeOH (5 mL) before the temperature was allowed to rise (NOTE: a rise in temperature above −50 °C before quenching leads to elimination and formation of colored products). The mixture was poured into brine (200 mL) and extracted with ether (500 mL). The organic phase was

(37) Eisner, J. *Ferroelectrics* **1972**, *4*, 213−219.
(38) Wada, Y.; Hayakawa, R. *Jpn. J. Appl. Phys.* **1976**, *15*, 2041−2057.
(39) Curtin, D. Y.; Paul, I. C. *Chem. Rev.* **1981**, *81*, 525−541.
(40) Liu, S. T. *Landolt-Börnstein, Numerical Data and Functional Relationships in Science and Technology*; Hellwege, K.-H., Ed.; Springer-Verlag: New York, 1979; Vol. 11/III, pp 471−494.
(41) Mighell, A. D.; Rodgers, J. R. *Acta. Crystallogr.* **1980**, *A36*, 321−326.
(42) Wilson, J. C. *Acta. Crystallogr.* **1988**, *A44*, 715−724.

dried (Na_2SO_4), and the solvents were evaporated on a rotary evaporator. The semicrystalline material was crystallized from boiling MeOH (500 mL) which gave **2** (8.23 g, 65%) as a colorless compound that was a mixture of isomers: mp 145−147 °C; ^{1}H-NMR (δ ppm, $CDCl_3$) 7.24−7.1 (m, 1H), 6.98−6.84 (m, 1H), 6.65−6.50 (m, 1H), 5.44−5.27 (m, 1H), 3.88−3.66 (m, 1H), 3.58−3.45 (m, 1H), 1.9−1.2 (m, 6H); ^{31}P-NMR (δ ppm, $CDCl_3$) −70 to −72 (m) Anal. Calcd for $C_{33}H_{36}PF_3O_6$: C, 64.27; H, 5.88. Found: C, 64.36; H, 5.73.

Tris(2-hydroxy-6-fluorophenyl)phosphine (3). (**2** (8 g, 13 mmol) was stirred in MeOH (800 mL) containing 37% HCl(aq) (16 mL) under argon. After 4 h the solution was evaporated to a volume of 20 mL. The mixture was then stirred with $CHCl_3$ (300 mL) and 1 M $NaHCO_3$(aq) (300 mL) under argon (NOTE: this is very important as the hydrochloride is the initial product). The clear organic phase was separated from the clear aqueous phase and dried (Na_2SO_4), followed by evaporation of the solvent. Crystallization from boiling toluene (100 mL) followed by careful addition of heptane (200 mL) under argon. The product was left to cryrstallize in the freezer. This gave **3** (4.32 g, 91%) as colorless crystals which were dried in a vacuum oven at 80 °C: mp 176.5−177 °C; ^{1}H-NMR (δ ppm, $CDCl_3$) 7.4−7.2 (m, 1H), 6.8−6.6 (m, 1H), 5.1 (s, 1H); ^{13}C-NMR (δ ppm, $CDCl_3$) 165.4 (dd, J_{C-F} = 245 Hz, J_{C-P} = 5.8 Hz), 161.0−160.6 (m), 130.6−130.4 (m), 110.46 (s), 109.31 (s), 106.39 (d, J = 25.8 Hz); ^{31}P-NMR (δ ppm, CD_3OD) −80 (q, J_{P-F} = 26 Hz). Anal. Calcd for $C_{18}H_{12}PF_3O_3$: C, 59.34; H, 3.32. Found: C, 59.94; H, 3.55.

4,8,12-Trioxa-12c-phospha-4,8,12,12c-tetrahydrodibenzo[*cd,mn*]-pyrene (4) (Phosphangulene). **3** (0.75 g, 2.06 mmol) was placed in a dry 50 mL round-bottomed flask under argon. *t*-BuOK (95%) (0.8 g, 6.18 mmol) was added, followed by dry NMP (20 mL). The solution acquired a slight tan color. The flask was then placed on an oil bath (200 °C) and stirred for 1 h, during which a precipitate formed and the color became dark brown. After cooling to room temperature, the mixture was poured into ether (200 mL), and the organic phase was then washed with water (2 × 150 mL). The organic layer was colorless, and all the colored products remained in the aqueous phase. The organic phase was dried (Na_2SO_4) and concentrated in vacuum to yield the pure phosphangulene with some NMP. The mixture was dissolved in boiling EtOAc (20 mL) and left to crystallize. Well-formed needles of **4** (0.54 g, 86%) were obtained (the product can be sublimed at 160 °C and 0.1 mmHg or at 200 °C and atmospheric pressure; in both cases, it takes 1 h): DSC showed melting in the interval 283−298 °C peak at 290.44 °C, 29.95 KJ mol^{-1}; mass spectra (EI$^+$) 304 *m/z*; ^{1}H-NMR (δ ppm, $CDCl_3$) 7.31−7.23 (m, 1H), 7.1−7.04 (m, 2H); ^{13}C-NMR (δ ppm, $CDCl_3$) 156.66 (d, J = 7.8 Hz), 130.37 (s), 115.29 (d, J = 1.2 Hz), 114.97 (d, 12.7 Hz); ^{31}P-NMR (δ ppm, $CDCl_3$) −133 (s). Anal. Calcd for $C_{18}H_9PO_3$: C, 71.05; H, 2.98. Found: C, 70.95; H, 3.00.

4,8,12-Trioxa-12c-oxyphospha-4,8,12,12c-tetrahydrodibenzo-[*cd,mn*]pyrene (5). **4** (0.15 g, 0.5 mmol) was dissolved in $CHCl_3$ (50 mL) and stirred vigorously overnight with 35% H_2O_2(aq) (4 mL) in a conical flask (100 mL) using a magnetical stirrer. The organic phase was separated and dried (Na_2SO_4). Evaporation and recrystallization from EtOAc gave **5** (0.1 g, 63%) as colorless crystals: mp 310−311 °C; mass spectra (EI$^+$) 320 *m/z*; ^{1}H-NMR (δ ppm, $CDCl_3$) 7.47 (t, 1H, J = 7.8 Hz), 7.18 (dd, 2H); ^{13}C-NMR (δ ppm, $CDCl_3$) 160.31 (s), 133.89 (s), 115.38 (d, J = 4.8 Hz), 110.32 (d, J = 108.4 Hz); ^{31}P-NMR (δ ppm, $CDCl_3$) −48(s) Anal. Calcd for $C_{18}H_9PO_4$: C, 67.50; H, 2.83. Found: C, 67.04; H, 2.46.

Statistical Analysis. All numerical results given with an indication of experimental error represent $\langle x\rangle \pm 2\sigma$, where $\langle x\rangle$ represents the *population mean* and 2σ represents *two standard deviations*.

Crystallographic Methods. The crystal structure of **4** was determined by X-ray crystallography using direct methods and least-squares refinement. Hydrogen atoms were found close to the observed positions and included in the final refinements. Data were collected on an Enraf Nonius CAD4 four-circle diffractometer. The absolute structure was confirmed by a Flack parameter of -0.01 ± 0.1. Crystallographic data are given in Table 1.

Powder diffraction was done using a STOE powder diffractometer scanning the interval $8° \le 2\theta \le 40°$ at a rate of 0.8° 2θ/min at 10 °C intervals in the range 30−200 °C (it was not possible to elevate the temperature above 200 °C as the material sublimed at a rate too fast to complete the scan). The peaks were fitted using a pseudo Voigt function having a Gauss/Lorenz ratio of 0.8. The zero point was fixed by assigning the 110 peak a 2θ value obtained from the calculated powder diffractogram. The following peaks were used in unit cell size determination: 110, 300, 220, 101, 021, 211, 330, 600, 520.

Table 1. Crystallographic Data for Phosphangulene (**4**)

formula	$C_{18}H_9PO_3$
formula wt	304.22
crystal system	trigonal
space group	*R*3*m*
Z	3
a, Å	16.6710(13)
b, Å	16.6710(13)
c, Å	4.2590(3)
α, β	90
γ	120
V, Å^3	1025.09(13)
ρ_{calc}, g cm^{-3}	1.478
crystal dimens, mm	0.4 × 0.05 × 0.05
T, K	293(2)
type of radiation	Cu Kα
μ, mm^{-1}	1.877
R(*F*), *Rw*(*F*2) all data	0.0234, 0.0570
GOF (on F^2)	1.057

Measurement of the Dipole Moment. The dipole moment was determined by measuring the capacitance at 21 °C of chloroform solutions of **4** with concentrations in the range 0.01−0.001 mol L^{-1}. The measurement of the capacitance was accomplished with an impedance analyzer from Hewlett-Packard (type 4192A LF). The dipole moment was obtained using the Onsager equation[43] and was found to be 3.3 ± 0.2 D.

Heat Capacity. The heat capacity of the crystal was estimated, from the calculated heat capacity for the gas phase molecule, to be C_p = 900 J kg^{-1} K^{-1}. The value for the solid is expected to be a little smaller than this value. The free molecule (gas phase) heat capacity was calculated with MOPAC and PM3.[44] Calculations were performed on a Power Iris Indigo and a Power Challenger from SGI.

Measurement of Dielectric Constants at Optical Frequencies. The relationship between the refractive indices and the relative permittivity was used to determine the values for the components of the dielectric permittivity tensor at optical frequencies. The material is uniaxial as is shown by the crystal structure. The refractive index n_3, for white light, was determined by means of a microrefractometer spindle-stage, using calcite as the refractometer crystal,[45] and found to be 1.575 ± 0.002. The refractive indices $n_1 = n_2$, are much higher than n_3; the crystal is thus optically negative like calcite. These components could not be determined directly because the crystals dissolved too rapidly in the refractometer oils available. In α-bromonaphthalene, however, the crystals dissolved at a rate sufficiently slow to allow interpolation in a sequence of microrefractometric measurements.[46] The path difference between the liquid and the crystal seen along the *c* axis gave the grain thickness, and the path difference between the liquid and the crystal seen perpendicular to the *c* axis then gave $n_1,n_2 - 1.657$, which gives $n_1,n_2 = 1.78 \pm 0.01$ for white light. The birefringence is thus 0.20. Using

$$n_i = \sqrt{\epsilon_{r,i}} \tag{1}$$

The relative dielectric permittivity tensor at optical frequencies can thus be written as

$$\epsilon_{i,j}^{\text{optical}} = \begin{pmatrix} 3.16 & 0 & 0 \\ 0 & 3.16 & 0 \\ 0 & 0 & 2.48 \end{pmatrix} \tag{2}$$

(43) Böttcher, C. J. F. *Theory of Electric Polarization*, 2nd ed.; Elsevier: Amsterdam, 1973; Vol. 1, pp 159−204.

(44) (a) Stewart, J. J. P. *J. Comput. Chem.* **1989**, *10*, 221. (b) Computational results obtained using the MOPAC program from MSI of San Diego, CA.

(45) Medenbach, O. *Fortschr. Mineral.* **1985**, *61*, 111−113.

(46) Beyer, H. *Theorie und praxis der interferenzmikroskopie*; Akademische Verlagsgesellschaft; Geest & Portig K.-G.: Leipzig, 1974.

At 35 GHz. The components of the relative dielectric permittivity tensor were measured by the microwave cavity perturbation method.[47,48] The *Q*-factor of a resonant cavity was measured when a crystal was placed in the resonant cavity with the crystallographic axis of interest aligned with the electrical field vector in the cavity. The frequency shift observed upon introducing the sample into the cavity is related to the dielectric constant in the direction aligned with the electric field as well as the appropriate filling and depolarization factors, which are estimated from the sample dimensions. The dielectric constants could thus be determined. The components were found to be ϵ_{11} and $\epsilon_{22} = 5.2 \pm 0.6$ and $\epsilon_{33} = 2.9 \pm 0.2$.

At 120 Hz and 1 kHz. The low-frequency isotropic relative permittivity was obtained by measuring the capacitance of a series of discs of the material prepared by compressing finely ground **4** under vacuum with a mechanical pressure of 400 kg m^{-2} to a density of 1425 $\pm$ 78 kg m^{-3}. The diameter of the discs were 13 mm, and their thicknesses varied from 0.1 to 0.4 mm. The values obtained were $\epsilon_{120\ Hz} = 4.7 \pm 0.8$ and $\epsilon_{1\ kHz} = 4.7 \pm 1.1$.

Pyroelectric Measurements. Several methods have been described for the measurement of the pyroelectric coefficients.[24,40,49−55] Since we were dealing with relatively small single crystals ($1 \times 0.4 \times 0.4$ mm^3), the only method that worked well was the temperature step method.[24] When subjecting the crystal to a step change in temperature, while measuring the potential appearing across a known capacitance, the pyroelectric coefficient can be obtained at any given temperature as the slope of the curve (or as the change in potential upon stepping) according to

$$\frac{\Delta P}{\Delta T} = p_3{}^T = \frac{C_{\text{total}}}{A}\frac{\Delta V}{\Delta T} \tag{3}$$

P being the polarization, $p_3{}^T$ the stress free pyroelectric coefficient, A the electrode area, C_{total} the total capacitance, V the voltage, and T the temperature. The charge generated was obtained by measuring the potential appearing across a capacitor (220 pF) placed in parallel with the sample. The potential measured across the sample and capacitor was buffered using a null configured electrometer operational amplifier AD549JH from Analog Devices. The temperature was controlled by means of a peltier element (MI1020T (0.9 W) from Marlow Industries Inc.) thermally connected to a heat sink (3.5 K W^{-1}) with heat conducting glue stuck to one side. The other side had a copper coating (0.01 mm) and was covered with a thin slice of mica (0.05 mm). Silver paste electrodes (Leitsilber 200 from DEMETRON) were applied to the crystal perpendicular to the *c* axis. Electrical connection to the null amplifier circuit was made with silver wire (0.05 mm Ø). The sample was placed in transistor heat transfer silicon grease on the mica-covered side of the peltier element. The sample/amplifier assembly was enclosed in a gold-plated brass box with gas inlet/outlet. The temperature was measured with an Al-Ni/Ni-Cr thermocouple. Data acquisition was achieved using a 12 bit A/D converter with digital output lines AX5210 from Axiom Inc. The digital output lines were used to control the temperature through a D/A converter (DAC0808LCN from National Semiconductor), driving the peltier element by means of a power operational amplifier (L165V from S G S Thompson).

Calibration of Pyroelectric Measurement Setup. In order to ensure that the measurements were correct the pyroelectric coefficients of reference samples were determined. Five $LiNbO_3$ samples with a known direction of polarization were used as reference materials. The samples were cut from plates of the material having a thickness of 0.5 mm with the *c* axis along the 0.5 mm dimension. Dimensions of individual samples typically measured $2 \times 2 \times 0.5$ mm^3 with the *c* axis perpendicular to the 2×2 mm^2 surface. The positive direction of polarization was known and connected to signal ground. When the temperature was raised the voltage which developed across the material had a positive sign with respect to signal ground. The capacitance of the samples had values of around 8.5 pF and the reference capacitor placed in parallel with the reference samples had a value of 15 nF. When the pyroelectric coefficient was measured as described in the section above, a value of -39 ± 3 μC m^{-2} K^{-1} was obtained at a temperature of 28 °C. This value is in good agreement with the literaure value[29] of -40 μC m^{-2} K^{-1} at a temperature of 25 °C.

Scheme 1

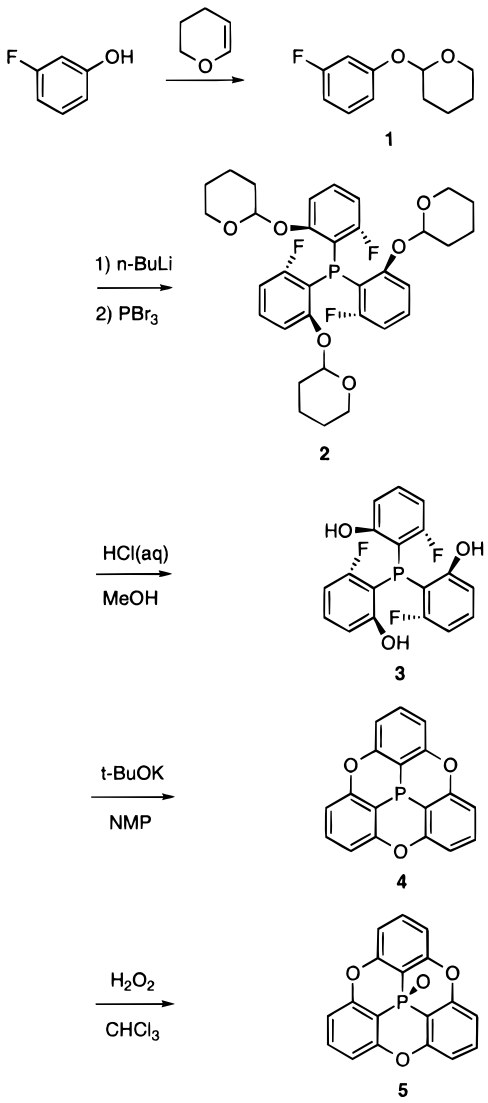

Thermogravimetric Measurements. The weight of a 6.603 mg sample was measured in the temperature range 20−200 °C. The rate of temperature change was set to 1 °C/min. At this rate of change of temperature, the weight loss became detectable at 127 °C. In order to show that sublimation took place at lower temperatures where the pyroelectric measurements were made, the weight of a 21.296 mg sample placed at a constant temperature of 100 °C was monitored over a 15 h period of time. During this period, 0.021 mg evaporated, corresponding to a rate of sublimation of 1.1×10^{-4} % (weight) min^{-1} at 100 °C. The measurements were made on a TGA51 thermogravimetric analyzer in conjunction with a Thermal Analyst 2000 from Dupont Instruments.

Results and Discussion

Compound **4** is a phosphine derived from triphenylphosphine. Its synthesis is fairly straightforward (Scheme 1), starting from commercially available 3-fluorophenol by reaction with 2,3-

(47) Buranov, L. I.; Shchegolev, I. F. *Probl. Tekh. Eksp.* **1971**, *2*, 171.
(48) Ong, N. P. *J. Appl. Phys.* **1977**, *48*, 2935−2940.
(49) Fabel, G. W.;Henisch, H. K. *Solid State Electron.* **1971**, *14*, 1281−1283.
(50) Hartley, N. P.; Squire, P. T.; Putley, E. H. *J. Phys.* **1972**, *E5*, 787−789.
(51) Gladkii, V. V.; Zheludev, I. S. *Sov. Phys. Crystallogr.* **1965**, *10*, 50−53.
(52) Chynoweth, A. G. *J. Appl. Phys.* **1956**, *27*, 78−84.
(53) Lang, S. B.; Steckel, F. *Rev. Sci. Instrum.* **1965**, *36*, 929−932.
(54) Shaulov, A.; Simhony, M. *Appl. Phys. Lett.* **1972**, *20*, 6−7.
(55) Gavrilova, N. D. *Sov. Phys. Crystallogr.* **1965**, *10*, 278−281.

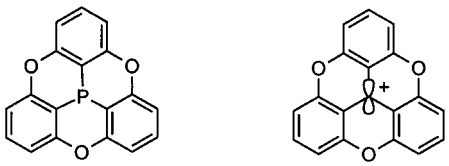

Figure 1. Molecular structure of phosphangulene (**4**), which is nonplanar, and the corresponding carbon compound, which in its cationic form is planar.

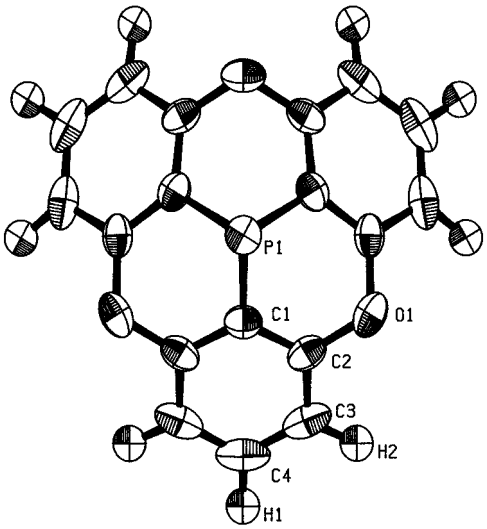

Figure 2. ORTEP drawing of phosphangulene (**4**). Only the asymmetric unit has been labeled.

dihydropyrane to give **1**. Selective lithiation in the 2-position and subsequent reaction with phosphoroustribromide gave **2**, which upon deprotection with hydrochloric acid gave **3**. Reaction of **3** with base and subsequent aromatic nucleophilic substitution by the phenolate ion gave the ring-closed product **4**. Compound **4** could be oxidized by hydrogen peroxide in chloroform. This gave the phosphine oxide **5**. It is possible to prepare tangible quantities of **4** (0.25−1.0 g scale possible). The corresponding carbon compound is planar in its cationic form.[56] Compound **4** is not planar, and therefore, its point symmetry is lower (Figure 1). It is this nonplanarity which gives rise to the appearance of a permanent dipole moment.

The crystal structure (Table 1) reveals that apart from being triangular (Figure 2) the shape of the molecule is similar to that of a Chinese hat (Figure 3) and also that these hats stack on top of one another forming a directed stack (Figure 3). An interesting point is that they stack in an eclipsed manner which allows the stacks to pack next to each other (Figure 4). The space group is rather unusual for an organic compound.[41,42] The crystal symmetry may be a consequence of the molecular symmetry of the molecule combined with the molecule's large aptitude toward stacking and packing. The particular arrangement of these molecular dipoles in the crystalline state thus gives the material the permanent polarization and the consequent pyroelectric properties.

The measurement of the pyroelectric properties in the temperature range 28−110 °C was accomplished by measuring the charge generation of a single crystal of the compound along the polar axis (the *c* axis). A known capacitance was connected in parallel (much larger than the capacitance of the electrical circuit (crystal, amplifier, and electrical connections)), and the electrical potential measured across this capacitance was taken as a measure of the amount of charge generated as the material underwent a step change of temperature (see the Experimental Section). This type of measurement results in an average value of the pyroelectric coefficient, p_3^T, over the temperature step region. The magnitude of the pyroelectric effect depends upon some of the physical properties of the molecule and of the material. The molecular dipole is responsible for the polarization. Since the volume of the crystal is unconfined during the course of the experiments, the pyroelectric coefficient obtained here is the pyroelectric coefficient at constant stress. It is thus composed of two different pyroelectric contributions[40]

$$p_n^T = p_n^S + e_{n\mu}^T \alpha_\mu^E \tag{4}$$

where *p, n, T, S, E, e,* μ, and α represent the pyroelectric coefficient, the polar axis, constant stress, constant strain, constant electric field, piezoelectric stress coefficient, tensor components, and thermal expansion constant, respectively. The second term represents the change in polarization per unit change of volume with temperature, which is due to the thermal expansion. This is known as the secondary pyroelectric coefficient. The first term is the primary pyroelectric coefficient, and when observed, this term is due to molecular or atomic movements within the crystal, leading to partial or full cancellation of the dipole moments. This does not necessarily lead to nor depend upon any change of volume of the unit cell. In both cases, the change in polarization leads to the generation of charges at the faces of the crystal perpendicular to the polar axis. When, in turn, the charge generation is considered across a resistance and a capacitance, be it the resistance and capacitance of the crystal itself or of the measuring device, the charge generation can be read as an electrical potential across the crystal. The magnitude depends upon the dielectric constant of the material across which the potential is read.

In order to predict the nature of the secondary pyroelectric properties of this material, or of any molecular material for that matter, a knowledge of the thermal expansivity, of the structure and of the molecular dipole is required. In the case of the prediction of primary pyroelectric coefficients, which depend upon the acoustical vibration modes of the material, it is necessary to consider the structural components as anharmonic oscillators and summing over the acoustical frequency band.[23] Their contribution to the heat capacity function of the material is proportional to the primary pyroelectric coefficient. Here we expect the primary effect to be negligible. In order, therefore, to predict the secondary pyroelectric properties, the thermal expansion was determined in the temperature range −95 to 200 °C, in part (−95 to 45 °C) using the four-circle diffractometer and in part (30−200 °C) using powder diffraction (Figure 5). The change in unit cell parameters (volume, axis lengths) upon thermal expansion clearly shows a linear relationship, keeping the results obtained by the two different methods separate from one another. The unit cell volume and unit cell parameters as a function of temperature are shown (Figure 5). Since no discontinuities in unit cell parameters are observed as a function of temperature, no abnormal dielectric behavior can be anticipated on this account. Furthermore DSC does not indicate that a phase transition takes place before the melting point is reached.

The expression for the polarization, *P*, is, when it is known that the axis of the molecular dipole, μ, and the *c* axis are collinear (their directions may be opposite),

$$P(T) = \frac{Z}{V(T)}\begin{pmatrix}0\\0\\\mu\end{pmatrix} \tag{5}$$

(56) Martin, J. C.; Smith, R. G. *J. Am. Chem. Soc.* **1964**, *86*, 2252−2256.

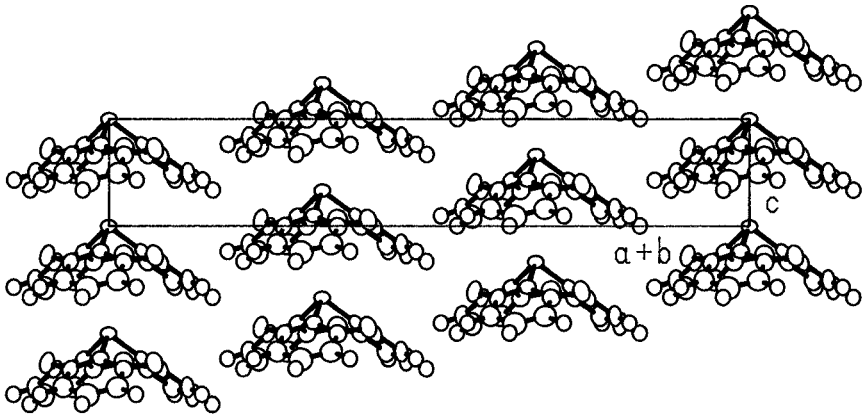

Figure 3. Drawing that emphasizes the manner in which the molecules stack on top of each other and how all the stacks point in the same direction.

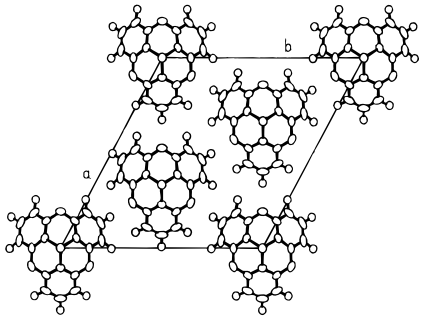

Figure 4. Drawing that shows the packing of the molecules in the *ab* plane.

where P, V, T, Z, and μ equal the polarization, volume (given as $V(T) = aT + b$), temperature, molecular entities per unit cell, and molecular dipole moment, respectively. The polarization at a given temperature can thus be calculated; at room temperature $P = 0.032$ C m^{-2}. Using the linear equation for thermal expansion and upon differentiating with respect to temperature, one obtains an expression for the secondary pyroelectric coefficient at a given temperature

$$\frac{dP(T)}{dT} = p_3(T) = -\frac{Z}{\left(aT^2 + 2bT + \frac{b^2}{a}\right)}\begin{pmatrix}0\\0\\\mu\end{pmatrix} \qquad (6)$$

A plot of the experimentally determined pyroelectric coefficient and of the pyroelectric coefficient obtained using the equation above shows a good similarity between the two at temperatures below 60 °C (Figure 6). At temperatures above 60 °C, however, the observed pyroelectric coefficient becomes nonlinear and increases rather rapidly in magnitude. This is due to sublimation of the material, the effect of which cannot be separated from the true secondary pyroelectric effect, since they both lead to a decrease in spontaneous polarization (or in effect, a decrease of molecular dipoles per unit volume). The fact that sublimation occurs and that this is solely responsible for the observed deviation from the calculated pyroelectric coefficient was quantified by thermogravimetric measurements (Figure 7). An obvious practical argument is that the material can be sublimed at 90 °C in a vacuum-sealed tube over 24 h. Any reaction with oxygen can be excluded as the material sublimes in open air without formation of any oxide as shown by phosphorous NMR of a sample sublimed in air. The rate of sublimation at 100 °C, determined by thermogravimetry, compares quite well to the rate of disappearance of molecular dipole moments obtained as the increase in the pyroelectric signal at 100 °C compared to the value of the pyroelectric signal at 28 °C.

The presence of ferroelectric properties would imply that the polarization of the material could be reversed. Possible mechanisms to achieve this are (a) a mechanism that would require the molecules to somehow undergo inversion either by inverting around the phosphorous atom or by rotating in the crystal or (b) a mechanism where the overall dipole moment is a result of intermolecular dipoles rather than intramolecular dipoles as expected. Inversion around phosphorous is highly unlikely first of all because phosphines generally do not invert as evidenced by the fact that optically active and optically stable phosphines can be made, indicating that the inversion barrier is too high for inversion in the temperature span where organic molecules are stable.[57] Further, inversion around phosphorous in the crystalline phase would imply that all the molecules invert at the same time in one concerted step since it would be impossible to invert just one molecule and place it inverted on its former site. This last statement also explains why rotation of the individual molecules in the crystal can be ruled out as a possible mechanism of ferroelectric behavior. In addition, such a mechanism would severely affect the magnitude of the structure factors, and even though the overall periodicity of the lattice is not disrupted, such a mechanism would affect the appearance of the X-ray powder diffractogram, an observation that has not been made. The last mechanism would require that the molecules were very polarizable, that two different distributions of electrons in the molecule or in between molecules were possible, and that each distrubution would result in a dipole moment with a direction opposite to the other such that the effective direction of polarization could be reversed. A way to establish whether the direction of polarization can be reversed is by establishing whether the field dependence of the polarization shows any hysteresis, a characteristic feature of ferroelectric materials.[58] Attempts were made to measure the field dependence of polarization by the Sawyer method.[59] The results were not conclusive because the sample capacitances that could be obtained ranged between 0.5 and 2 fF. These capacitance values were found to be much too small for practical purposes. Even though no numerical information on the field dependence of the polarization could be obtained, it is concluded that compound **4** does not exhibit ferroelectric behavior, mainly because the molecule itself does not have any molecular structural features which suggest that the molecule can alter its conformation nor

(57) Horner, L.; Winkler, H.; Rapp, A.; Mentrup, A.; Hoffmann, H.; Beck, P. *Tetrahedron. Lett.* **1961**, 161.
(58) Jona, F.; Shirane, G. *Ferroelectric Crystals*; Pergamon Press Inc.: Oxford, U.K., 1962; pp 1−23.
(59) Sawyer, C. B.; Tower, C. H. *Phys. Rev.* **1930**, *35*, 269−273.
(60) Brandrup, J.; Immergut, E. H. *Polymer Handbook*, 3rd ed.; John Wiley & Sons: New York, 1989; pp V51−V54.

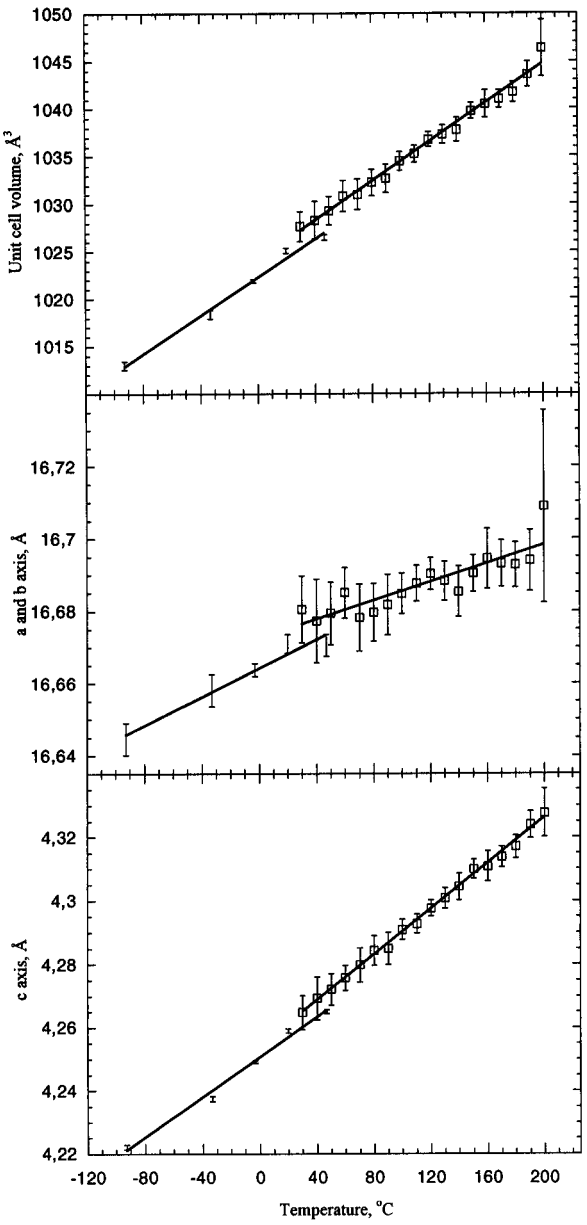

Figure 5. Plots as a function of temperature of the unit cell volume (above), the *a*,*b*-axis length (middle), and the *c*-axis length (below). The values in the lower part of the temperature range were obtained using a four-circle diffractometer (CAD4) on a single crystal, and the higher temperature range values were obtained using powder diffraction (STOE).

exhibit any polarization properties much different from those of its constituent phenyl rings taken individually.

The assignment of the direction of the molecular dipole moment, with respect to the molecule itself, can be made when the relationship between the physical morphology of the crystal and the crystal structure is known (Figure 8) and when, at the same time, the orientation of the crystal during measurement of the pyroelectric coefficient is known. The physical morphology of the crystals is similar to the shape of a pencil sharpened at one end. This makes it very easy to orient the crystals with the positive *c* axis in the direction of interest when performing measurements on the crystals. The sign of the secondary pyroelectric coefficient is negative because linear expansion leads to a decrease in polarization.

The experimentally observed sign of the pyroelectric response (Figure 9) depends upon the orientation of the crystal during measurement, and it is observed that, upon increasing the

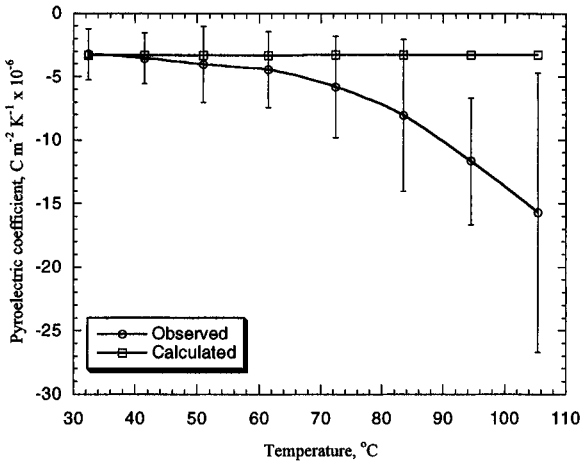

Figure 6. Calculated secondary pyroelectric coefficient as a function of temperature obtained by combination of eq 6 and the linear expansion from Figure 5. This is compared to the experimentally observed pyroelectric response that shows an increase in magnitude at increased temperature.

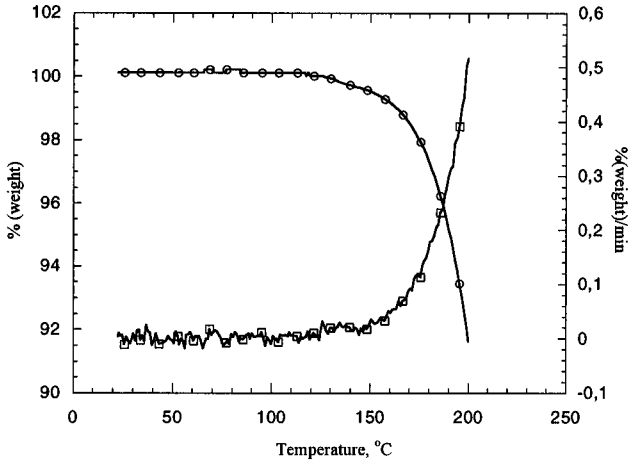

Figure 7. Result of thermogravimetric measurements in the temperature range 20−200 °C. At a scan rate of 1 °C/min, sublimation becomes detectable at 127 °C. The upper curve represents the weight of the sample in percent of the initial sample weight. The lower curve represents rate of loss of material per minute. Weight loss given in percent of the initial sample weight per minute.

temperature, the pointed end of the crystal acquires an electrical potential higher than that of the flat end. We know from the structure/morphology relationship (Figure 8) that at the pointed end all the concave sides of the molecules are exposed. The appearance of positive charges at the electrode at the pointed end when subjecting the crystal to a temperature rise (Figure 10) implies that the pointed end of the crystal must have the negative charge. These results thus show that the molecular dipole moment is directed from the concave to the convex side of the molecule (following the convention for the direction of the molecular dipole moment from − to +). In other words, the negative end of the molecule is the benzene rings and the positive end of the molecule is at the phosphorous atom (Figure 11). To further substantiate these findings, an identical experiment with $LiNbO_3$ as the pyroelectric sample with a known direction of polarization was carried out. This showed that the direction of polarization could be found and further that the literature value for the pyroelectric coefficient of $LiNbO_3$ could be reproduced with the experimental setup.

It is noticeable that the dielectric permittivity tensor has the largest components perpendicular to the *c* axis. This is in good agreement with the notion that the benzene rings are very

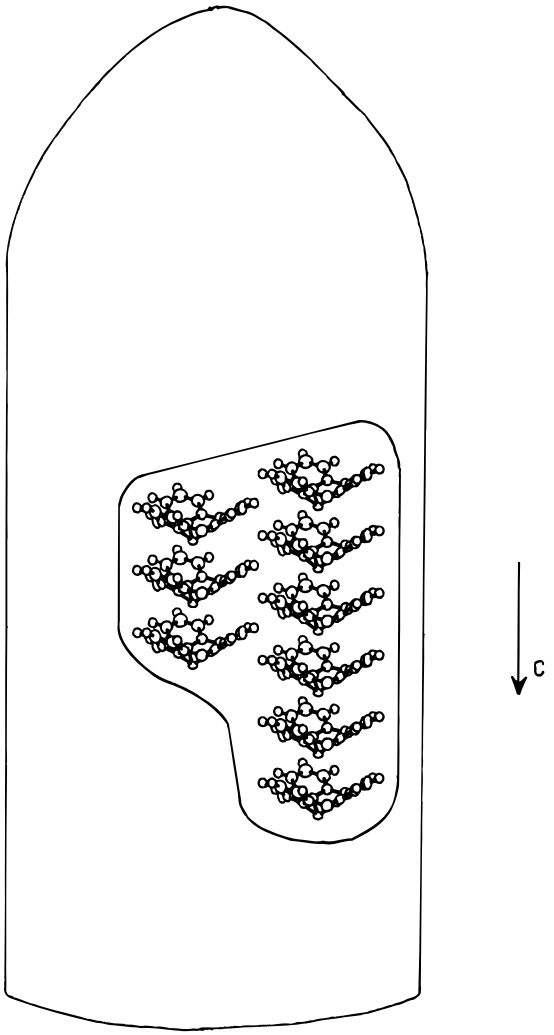

Figure 8. Drawing showing the orientation of the molecules with respect to the physical morphology of a typical crystal.

polarizable in the plane of the ring. The planes of the benzene rings are (due to the hat shape of the molecule and the orientation of the molecules in the unit cell) forming an angle with the *c* axis. The polarizable benzene rings thus have a component in the *c* direction and a much larger component in the *a*, *b* direction. The only significant contribution to the permittivity at room temperature is thus believed to be electronic in nature. The fact that the magnitude of the relative permittivity is smallest in the *c* direction is a great advantage when considering the performance of a pyroelectric detector system. When evaluating a material for potential use in a detector system, the detectivity merit factor is derived. The detectivity merit factor, M_r, for a pyroelectric material, can be expressed as a function of its dielectric permittivity, heat capacity, density, and of course its pyroelectric coefficient at the given temperature:[2]

$$M_r = \frac{p_n(T)}{\epsilon_o \epsilon_r c_p \rho} \tag{7}$$

The units are $m^2\ C^{-1}$ and express the signal voltage obtainable with a given material when multiplied with the energy absorbed at the surface:

$$\text{signal voltage (J C}^{-1}) = M_r\ (\text{m}^2\ \text{C}^{-1}) \times \text{energy (J m}^{-2}) \tag{8}$$

When compared to other known materials, phosphangulene (**4**)

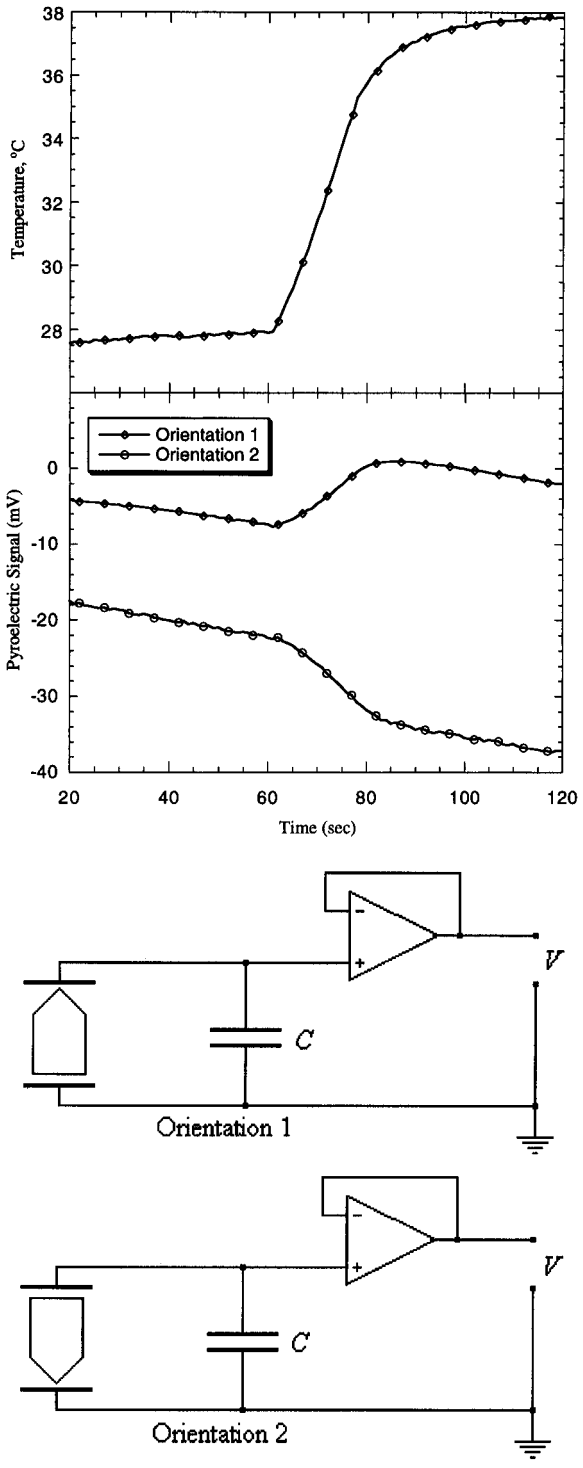

Figure 9. Plots of the step temperature change (top graph), the corresponding pyroelectric response when orientating the crystal with the flat end electrically connected to ground (orientation 1, middle graph), and the pointed end electrically connected to ground (orientation 2, bottom graph). Schematic drawings of the electrical setups and the orientations are shown below the graphs.

was found to be comparable in performance to many of the known pyroelectric matarials but also lower in performance when compared to the most yielding materials such as PVDF, TGS, and Li_2SO_4 hydrate. A few examples of merit factors for various materials are given at 25 °C (Table 2). In infrared detection, the interest is to have a material which responds to small variations in temperature (small differences in energy), the smaller the better. The properties outlined above are important when considering the magnitude of the pyroelectric voltage obtainable with a given material. The use of phos-

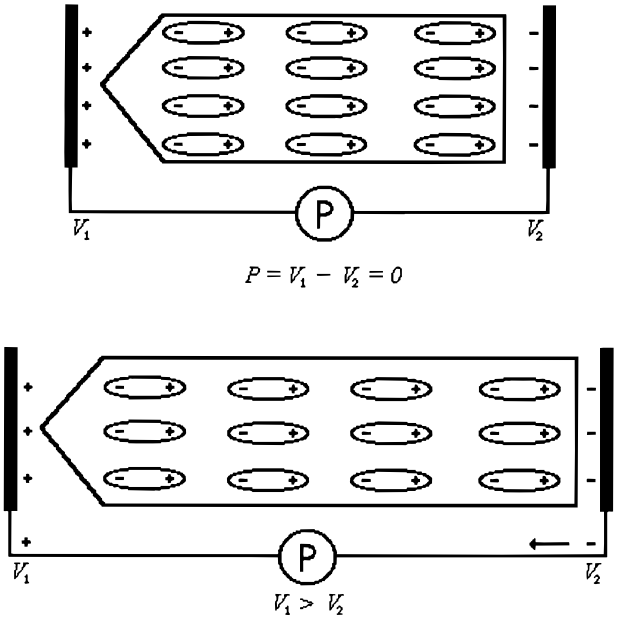

Figure 10. Illustration of the observed pyroelectric response when a crystal is subject to a thermally induced volume expansion. Above, the crystal is in thermal and electrical equilibrium at one temperature. Below, thermal equilibrium has been reached at a new and higher temperature. The material has expanded, and an increase in volume is seen. Electrical equilibrium is, however, not achieved, and charges are consequently observed at the electrodes (thick vertical lines). The orientation of the dipoles in the dielectric between the capacitor plates is thus deduced from the sign of the potential difference.

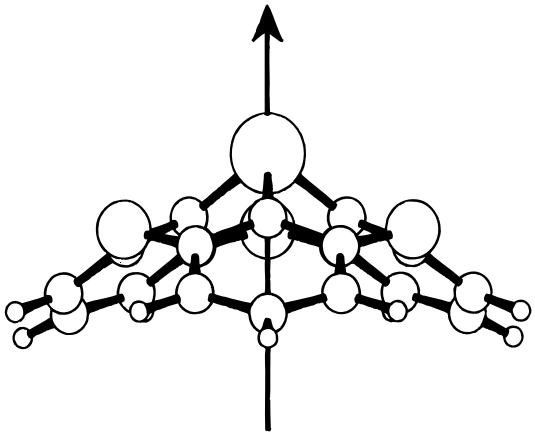

Figure 11. Drawing of the molecule together with the unambiguously assigned direction of the molecular dipole moment with respect to the molecular geometry (following the convention that the direction is toward the positive charge).

phangulene in a detector system, although a possibility based on the value of the merit factor, is essentially problematic because of the significant vapor pressure of the material at temperatures just above room temperature.

Table 2. Comparison of Phosphangulene (**4**) with Some Known Materials (at 298 K)

material	Pn[a] ($C\ m^{-2}\ K^{-1} \times 10^{-6}$)	ϵ_r	c_p ($J\ kg^{-1}\ K^{-1}$)	ρ ($kg\ m^{-3}$)	M_r ($m^2\ C^{-1} \times 10^{-2}$)
4[b]	3.2	2.9	1000	1478	8.4
PVDF[c]	27−40	8.4−13.5	806	1750−1800	23−25
$LiNbO_3$	40[d]	28[e]	635[e]	4640[e]	5.4
$LiTaO_3$[e]	176	43	430	7450	14.4
TGS[f]	280	43	1500	1700	28.8
$Li_2SO_4H_2O$[e]	100	8	400	2050	172
SBN[g]	600	400	440	5326	7.2
La:SBN[g]	1170	1630	490	5328	3.1

[a] Numerical value only. [b] This work. [c] Data from ref 60. [d] Data from ref 29. [e] Data from ref 2. [f] Data from ref 7. [g] Data from ref 4.

Conclusions

Phosphangulene (**4**) was synthesized and its crystalline structure determined. It was found to belong to a rare space group and to have pyroelectric properties, the nature of which were characterized in the temperature region 20−110 °C. The thermal expansivity in the temperature region −95 to 200 °C was also determined and used to predict the nature of the secondary pyroelectric properties using the value of the molecular dipole moment measured in solution. The success of this approach is due to the fact that the molecule has a locked conformation. Only when the conformation is the same in solution as in the solid state can the assumption be made that the dipole moment is similar in magnitude both in the solid state and in solution. The direction of the molecular dipole moment with respect to the molecule itself was determined. The molecular heat capacity was calculated. The refractive indices and the dielectric constants at optical frequencies, at 35 GHz, and the isotropic dielectric constant at low frequencies (120 Hz and 1 kHz) were determined. The material was considered for potential use in infrared detection and compared with that of known materials. It was found to be comparable in performance to known materials but to have a significant vapor pressure just above room temperature, making an application difficult.

Acknowledgment. We thank D. Micheelsen, Ole V. Petersen, Mikkel Jørgensen, Per Michael B. Johansen, and Finn W. Poulsen. Special thanks to Klaus Bechgaard for reading this manuscript as well as making this work possible.

Supporting Information Available: Tables of fractional coordinates, equivalent isotropic and anisotropic thermal parameters, bond lengths, bond angles, and unit cell parameters in the temperature range −93 to 200 °C (7 pages). See any masthead page for ordering and Internet access instructions.

JA962023C